SCIENCE CHINA
Chemistry

• ARTICLES •

September 2015 Vol.58 No.9: 1471–1477
doi: 10.1007/s11426-015-5430-x

Coil to globule transition of homo- and block-copolymer with different topological constraint and chain stiffness

Wei Wang, Yanchun Li & Zhongyuan Lu*

State Key Laboratory of Supramolecular Structure and Materials; Institute of Theoretical Chemistry, Jilin University, Changchun 130023, China

Received October 30, 2014; accepted December 1, 2014; published online May 22, 2015

In this paper, we present the coil-to-globule (CG) transitions of homopolymers and multiblock copolymers with different topology and stiffness by using molecular dynamics with integrated tempering sampling method. The sampling method was a novel enhanced method that efficiently sampled the energy space with low computational costs. The method proved to be efficient and precise to study the structural transitions of polymer chains with complex topological constraint, which may not be easily done by using conventional Monte Carlo method. The topological constraint affects the globule shape of the polymer chain, thus further influencing the CG transition. We found that increasing the topological constraint generally decreased CG transition temperature for homopolymers. For semiflexible chains, an additional first-order like symmetry-broken transition emerged. For block copolymers, the topological constraint did not obviously change the transition temperature, but greatly reduced the energy signal of the CG transition.

coil-to-globule transition, topological constraint, chain stiffness, molecular dynamics

1 Introduction

Macromolecules with circular and knotted conformations are popular in nature. Circular DNA has been found in viruses [1,2], and cyclic protein—the cyclotide, has been found in plants [3,4]. It has been found that the knotted proteins cover more than 1% of the Protein Data Bank entries [5]; and DNA molecules with topological knots can be detected in a reaction mixture of circular DNA and type II DNA topoisomerase [6,7]. These studies showed that knotted structures may play a very important role in life.

Synthetic cyclic and knotted polymers are of great interest in the investigation of topological effects on their physical properties. They serve as simplified models for their native counterparts, thus inherent physical behaviors of cyclic and knotted polymers can be thoroughly investigated. Many efforts have been made to synthesize and characterize cyclic polymers [8–10]. Recently, the knotted polymers—knotted polystyrene (PS) rings have also been synthesized and characterized [11,12]. The universal properties of circular and knotted polymers such as the entropic properties [13,14], the geometrical properties [15–17], the scaling behavior [14,18], and the diffusion behavior [19–22] have been fully investigated.

The collapse of a single polymer chain from an extended coil state in a good solvent to a compact globule state in poor solvent is called the coil-to-globule (CG) transition. A lot of work had been done to elucidate the influence of chain length, chain hydrophobicity difference, chain stiffness, and confinement on the CG transition of polymer chain [23–35]. However, studies on CG transition of polymers with topological constraints are still scarce, even though it is extremely important to understand the configuration transitions of their counterparts in nature [36–38]. To avoid time-consuming calculations of the topological invariant, a molecular dynamics (MD) method with suitable en-

*Corresponding author (email: luzhy@jlu.edu.cn)

© Science China Press and Springer-Verlag Berlin Heidelberg 2015

hanced sampling technique seems to be a straightforward candidate to solve this problem.

In this work, we studied the CG transitions of both homopolymers and regularly distributed block copolymers with different stiffness and topological constraints by using a novel enhanced sampling method—integrated tempering sampling (ITS) method [39–41] implemented in GPU MD code GALAMOST [42]. The stiffness is considered in this study owing to the fact that most macromolecules in nature are semiflexible and stiffness itself is also an important factor influencing CG transition [23,24,31].

This paper is organized as follows: in Section 2, the models of polymers with different topological constraints are described. The ITS method will be briefly introduced in Section 3, in which the main idea and the most important formulae are listed. The simulation details are illustrated in this section. The results and discussion are presented in Section 4, followed by the conclusions in Section 5.

2 Simulation models

In this study, four types of polymer chain topologies were considered, i.e. the circular type, the 3_1 knotted type, the 4_1 knotted type and the linear type for comparison. Common bead-spring models were used to describe both homopolymers and regularly distributed block copolymers. For homopolymers, the chain was composed of A type beads only, which were colored green (Figure 1). For block copolymers, the whole chain is composed of blocks of A and B type beads. We attributed that the A type beads were more hydrophobic and the B type beads were more hydrophilic, and B type beads were colored red (Figure 1). The chain length was set as N=40 for better comparison between different models. The model for homopolymers was denoted as A_{40}, and the model for block copolymers was denoted as $(A_5B_5)_4$.

Lennard-Jones potential was used between non-bonded beads with σ=1.0 and ε=1.0 (which, together with bead mass $m\equiv$1.0, are taken as the units in this study):

$$U_{\mathrm{LJ}}(r)=\begin{cases}4\varepsilon\left[\left(\dfrac{\sigma}{r}\right)^{12}-\left(\dfrac{\sigma}{r}\right)^{6}\right], & r\leqslant r_{\mathrm{cut}}\\ 0, & r>r_{\mathrm{cut}}\end{cases} \tag{1}$$

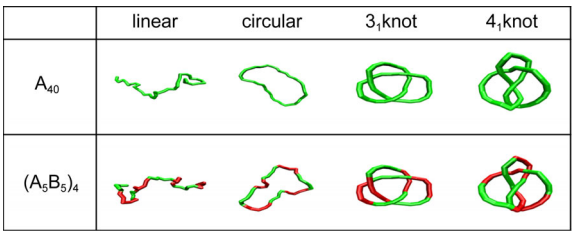

Figure 1 The models of the homopolymers and block copolymers with four types of topology.

with r_{cut} being set to 3.0 in our simulations.

The bonds were described by finite extensible nonlinear elastic (FENE) potential:

$$U_{\mathrm{FENE}}(r)=\begin{cases}-\dfrac{1}{2}k_{\mathrm{FENE}}r_0^2\ln\left(1.0-\dfrac{r^2}{r_0^2}\right)+U_{\mathrm{WCA}}, & r\leqslant r_0\\ \infty, & r>r_0\end{cases} \tag{2}$$

$$U_{\mathrm{WCA}}(r)=\begin{cases}4\varepsilon_{\mathrm{WCA}}\left[\left(\dfrac{\sigma_{\mathrm{WCA}}}{r}\right)^{12}-\left(\dfrac{\sigma_{\mathrm{WCA}}}{r}\right)^{6}\right], & r\leqslant 2^{\frac{1}{6}}r_{\mathrm{cut}}\\ 0, & r>2^{\frac{1}{6}}r_{\mathrm{cut}}\end{cases} \tag{3}$$

where r_0 is the bond extension parameter, k_{FENE} is the force constant, and r is the instantaneous bond length. To be consistent with previous work [35,41], we set σ_{WCA}=1.05, $\varepsilon_{\mathrm{WCA}}$=1.0, r_0=1.5, and k_{FENE}=40.

Chain stiffness was controlled by the bending potential between two successive bonds, which takes the form:

$$U_{\mathrm{bend}}=\frac{1}{2}k(\theta-\theta_0)^2 \tag{4}$$

where θ is the bond angle between two adjacent bond vectors and θ_0 is the equilibrium bond angle, which was taken as 180°. k is the bending force constant and varies from 0 to 8 to represent different chain stiffness.

To describe different hydrophobicity of A and B type beads in block copolymers, we used Lennard-Jones potential with different energy parameter ε to characterize the strength of short-range attractive interaction. To describe more hydrophobic A type beads, we set ε to 1.0, i.e., ε_{AA}=1.0. To describe more hydrophilic B type beads, ε was set to 0.2, i.e., $\varepsilon_{\mathrm{BB}}$=0.2. To represent the incompatibility between A and B beads, the interaction parameter between them was set the same as that between B type beads, i.e., $\varepsilon_{\mathrm{AB}}=\varepsilon_{\mathrm{BB}}$=0.2.

3 Simulation method

The integrated tempering sampling method is a novel enhanced sampling method based on generalized ensemble to generate a distribution covering a broad range of energies. Here we only give a brief introduction to this method, since details of the calculation process have been introduced in previous work [35,41]. The main idea in the ITS method is to use a biased potential generated from the combination of a series of canonical energy distributions. This allows a free walk in the energy space in a desired temperature range. In brief, the generalized distribution function $W(r)$ is defined as a summation over k temperatures:

$$W(r)=\sum_k n_k \mathrm{e}^{-\beta_k U(r)} \tag{5}$$

where U is the potential energy, $\beta_k=1/k_BT_k$ (k_B is Boltzmann constant, and T_k is the k-th temperature), and n_k is the weighting factor representing the contribution from each temperature β_k. The biased potential U' is defined by:

$$e^{-\beta U'(r)} \equiv W(r) \tag{6}$$

Thus,

$$U'(r) = -\frac{1}{\beta}\ln\sum_k n_k e^{-\beta_k U(r)} \tag{7}$$

The biased force F_{bias} is simply the force in conventional MD simulations, F, with a pre-factor:

$$F_{bias} = -\frac{\partial U'}{\partial r} = -\frac{\partial U'}{\partial U}\frac{\partial U}{\partial r} = \frac{\sum_k n_k\beta_k e^{-\beta_k U(r)}}{\beta\sum_k n_k e^{-\beta_k U(r)}}F \tag{8}$$

Thus the ITS method can be easily implemented in any MD code by slightly modifying the force subroutine. The thermodynamic properties of any canonical ensemble whose temperature (β_i) is in the desired range can be calculated from the generalized ensemble by using reweighting:

$$\langle A\rangle_{\beta_i} = \frac{\int A(r)e^{-\beta_i U(r)}dr}{\int e^{-\beta_i U(r)}dr} = \frac{\int \frac{A(r)e^{-\beta_i U(r)}}{W(r)}W(r)dr}{\int \frac{e^{-\beta_i U(r)}}{W(r)}W(r)dr} = \frac{\left\langle \frac{A(r)e^{-\beta_i U(r)}}{W(r)}\right\rangle W}{\left\langle \frac{e^{-\beta_i U(r)}}{W(r)}\right\rangle W} \tag{9}$$

Typical computational procedure of ITS simulation is therefore: (1) determine the interested temperature range; (2) choose a set of temperatures in the desired range determined in step (1) and run several relatively short time conventional MD simulations. Then obtain the relation between potential energy and temperature by interpolation; (3) determine the ITS temperature distribution and the corresponding weighting factors n_k as described in [41]; (4) use the parameters generated in step (2) and (3) to perform ITS simulation, which is essentially a conventional MD simulation using biased force; (5) after ITS simulation, the canonical ensemble properties can be calculated by using the reweighting technique.

Nosé-Hoover thermostat was adopted in our ITS simulations. The potential energies at different temperatures are first obtained by 1×10^6 steps MD simulations at 8 temperatures in the range of 0.5–5.0 for both homopolymers and block copolymers. The dependence of potential energy on temperature is used to estimate the weighting factors n_k [41]. We then perform 1×10^9 steps ITS simulations with GALAMOST package [42] for each model, and the data were recorded every 1×10^3 steps. Using a single ITS simulation trajectory, we can obtain thermodynamic properties of the system at any temperature in the temperature range by reweighting.

4 Results and discussion

We calculated the radius of gyration (R_g) of the chain and its derivative as well as the specific heat (C_v) as structural and thermodynamic indicators, respectively, to characterize CG transitions. The R_g was defined as:

$$\left\langle R_g^2\right\rangle = -\frac{1}{2N^2}\left\langle\sum_{i=1}^{N}\sum_{j=1}^{N}\left|r_{ij}^2\right|\right\rangle \tag{10}$$

and the C_v was defined as:

$$C_v = \frac{\partial U}{\partial T} = \frac{\left\langle E^2\right\rangle - \left\langle E\right\rangle^2}{k_BT^2} \tag{11}$$

The dependence of both R_g and C_v on temperature for homopolymers with different topologies and stiffness are shown in Figures 2 and 3, respectively.

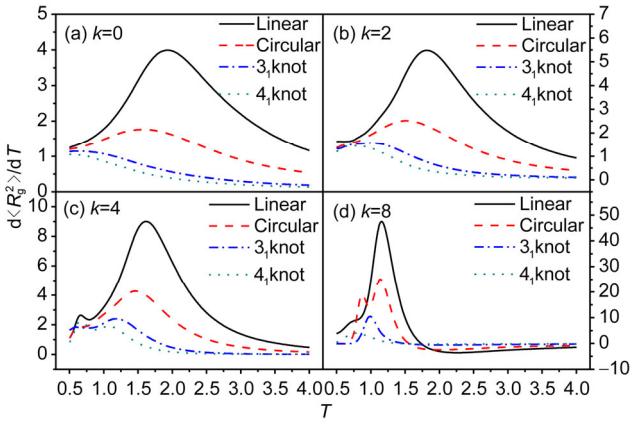

Figure 2 The first derivative of the mean square radius of gyration versus temperature ($d\langle R_g^2\rangle/dT$) for all types of homopolymer chains.

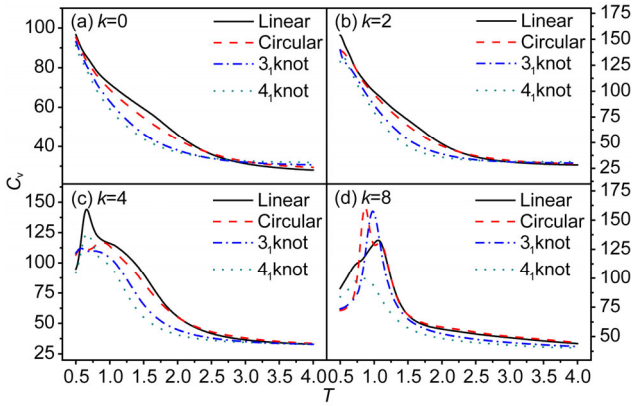

Figure 3 The specific heat (C_v) versus temperature for all types of homopolymer chains.

From Figure 2, we can observe peaks in the derivative of R_g for most of the curves, which clearly indicate the structure changes corresponding to CG transitions.

We can also clearly see from Figure 2 that the homopolymers with four types of topologies show different structural response with decreasing temperature. The topological constraints reduce the extension of the polymer, thus the signal of structural indicator is weaker for polymer chains with constraints than that of the linear polymer chains. Moreover, we can see that the CG transition temperature is moving to the lower temperature region with enhancing constraints. In cases with k=0, the CG transition temperature of 3_1 knot and 4_1 knot even moves out of the temperature range. This phenomenon is consistent with experimental results: Θ-temperature of ring polystyrene was found to be lower than that of linear polystyrene [43–45]. It can be explained by considering effective topological interaction of ring polymers in the framework of excluded-volume theory [46–48], which shows that for ring polymers, the topological constraints and the excluded volume interactions have similar effects. Thus increasing complexity of the topological constraint implied an additional effective contribution to the excluded volume of the monomers. It explains why we can observe lower CG transition temperature for circular and knotted polymers in our simulations. Figure 2 also shows that the CG transition temperature decreased with increasing chain stiffness, and correspondingly the transition peak turned to be sharper, in consistent with previous works [23,24]. Moreover, another peak showed up in the lower temperature region for most of the chains. Figure 3 shows that the CG transition peak also showed up in the C_v curves for the chains with higher stiffness, implying that the transition turns to be first order in these cases. To clarify the origin of the additional peak, we focused on the change of shape of the polymer chains in the process of CG transition.

The shape of a polymer chain can be characterized by the inertial properties [16,17,32]: for example, by calculating three principal moments of inertia for a given configuration of the polymer chain. We used an ellipsoid with the same principal moments of inertia to represent the shape of the polymer configuration. The moments of inertia tensor can be defined as:

$$T_{ij} = \frac{1}{2N^2}\sum_m\sum_n\left(x_n^i - x_m^i\right)\left(x_n^j - x_m^j\right) \quad (i=1,2,3;\ j=1,2,3) \tag{12}$$

where m, n denote the number of the beads, i, j denote the dimension of the coordinates, thus x_n^i means the i-th coordinate of the n-th bead and N=40 is the number of beads in a polymer chain. Three eigenvalues, λ_1, λ_2, and λ_3, were obtained after diagonalizing the matrix with elements defined by Eq. (12). In the following, we denoted $\lambda_1 \geqslant \lambda_2 \geqslant \lambda_3$. We used an invariant shape descriptor, i.e., the relative shape anisotropy κ, to characterize the symmetry of the polymer shape, which is defined as:

$$\kappa = 1 - 3\frac{\lambda_1\lambda_2 + \lambda_2\lambda_3 + \lambda_1\lambda_3}{\left(\lambda_1 + \lambda_2 + \lambda_3\right)^2} \tag{13}$$

This parameter has values between 0 and 1. It reaches 1 for an ideal linear chain and drops to 0 for highly symmetric chain configuration. For planar symmetric chain configuration, κ approaches to the value of 0.25. Another shape descriptor is the asphericity parameter b, which measures the deviation of a shape from spherical symmetry, defined as:

$$b = \lambda_1 - \frac{1}{2}\left(\lambda_2 + \lambda_3\right) \tag{14}$$

These two shape descriptors were also calculated at every temperature, and the results are shown in Figures 4 and 5, respectively.

From both figures we can clearly see that the additional peak appears at the lower temperature especially in the case with k=4. It actually indicates a structure transition from chain configuration with high symmetry to that of lower

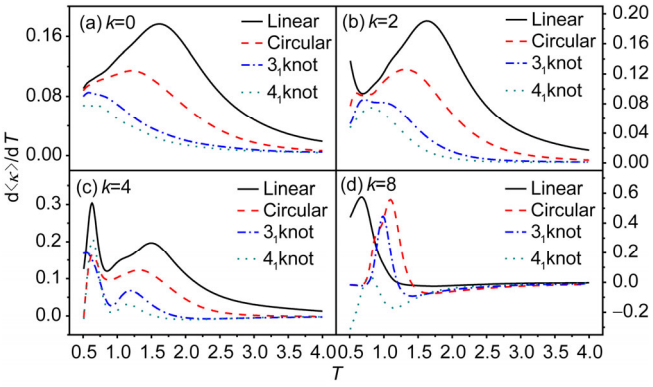

Figure 4 The first derivative of the relative shape anisotropy versus temperature (d⟨κ⟩/dT) for all types of homopolymer chains.

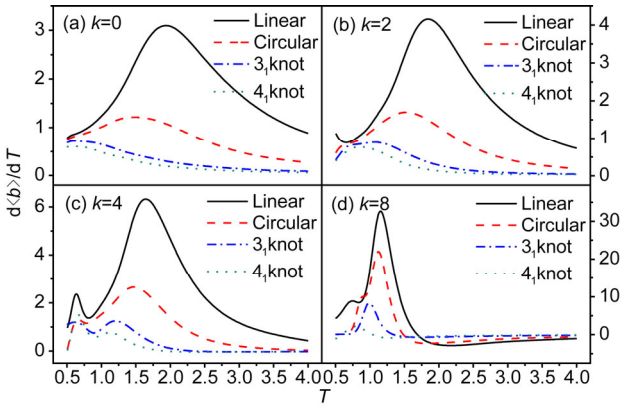

Figure 5 The first derivative of asphericity parameter (d⟨b⟩/dT) versus temperature for all types of homopolymer chains.

symmetry. This symmetry-broken transition normally corresponded to peaks in energy signal, indicating that this additional transition is first order like. However, this transition is not liquid-crystal (LC) transition judging from the structure of the chain. The peak of LC transition is supposed to appear at a much lower temperature, which is beyond this research.

To further elucidate the symmetry-broken transition, we take 3_1 knot homopolymer chain as an example. Typical configurations of 3_1 knot homopolymer are illustrated in Figure 6. It should be noted that Figure 6(b, c) correspond to semiflexible 3_1 knot homopolymer at different temperatures, and the chain configuration transition between these structures contributes to the additional peak shown in Figure 5(c).

The phase diagram for 3_1 knot homopolymer based on the simulation results is shown in Figure 7. Typical chain configurations as illustrated in Figure 6 can be seen in the low temperature region of the phase diagram. The borders between different regions correspond to the transition peaks in Figures 4 and 5.

For block copolymer chains, the structural indicator R_g and the thermodynamic indicator C_v for characterizing CG transition are calculated at different temperatures. The results are shown in Figure 8.

From Figure 8 we can see that, the CG transition behavior of block copolymer chains was relatively simpler than that of homopolymer chains. The topological constraints also reduced the extension of the block copolymer chains, thus the signals of both structural and energy indicators were suppressed. The CG transition temperature of block copolymers also decreased with enhancing topological constraint, but the decrease was not so obvious. Moreover, for block copolymers, there was no additional transition peak at lower temperatures as the chain stiffness increased. This means that there was only one CG transition for block copolymers, without any structure transition in globule state as in the cases of homopolymers (cf. Figure 7). Figure 8 also shows that the CG transition of block copolymers was first-order like [25,26,33]. Increasing chain stiffness enhanced the CG transition, as indicated by the peak heights in the C_v curves.

Now we focused on the globule structures of both homopolymer and block copolymer chains at T=0.5. To find the structural difference between these polymers at low

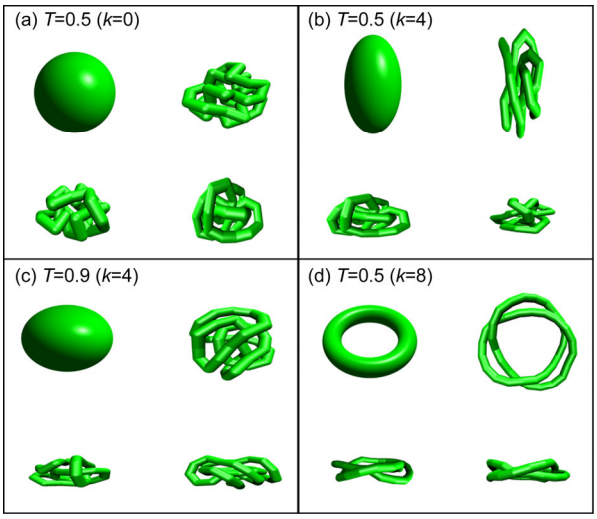

Figure 6 Typical configurations of 3_1 knot homopolymer chain. (a) Spherical; (b) rod-like; (c) flat prolate; (d) toroid. The left-up pictures in each subfigure shows the schematic, the other three pictures in each subfigure show the chain configuration viewed along the three principal axes of the moments of inertia.

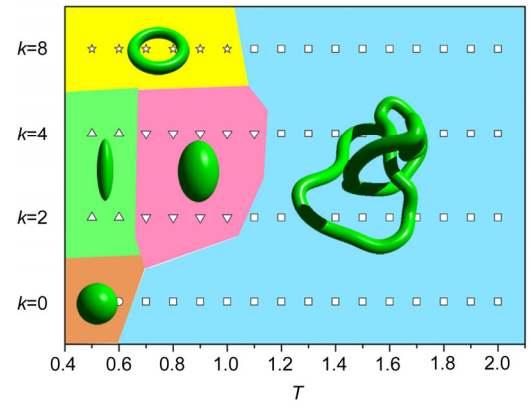

Figure 7 The phase diagram of 3_1 knot homopolymer. The blue region on the right corresponds to the coil state, and the regions on the left correspond to globule state with different shapes of the globule. The orange, green, pink, and yellow region represents the spherical, rod-like, flat prolate and toroidal shape, respectively.

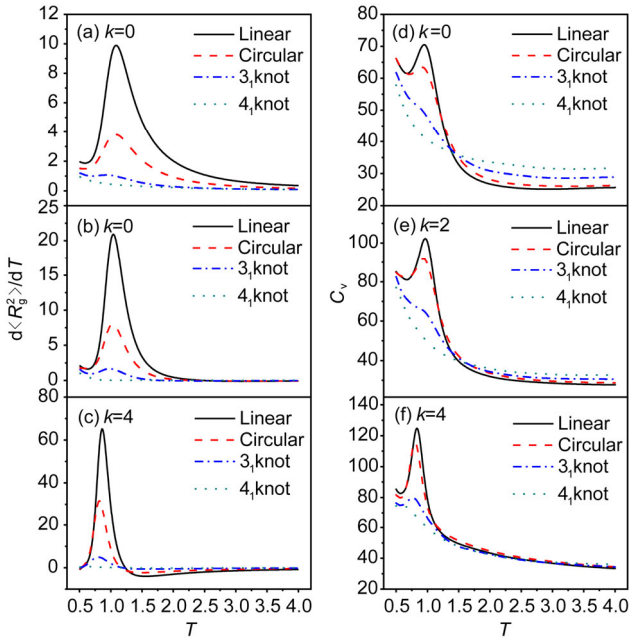

Figure 8 The first derivative of the mean square radius of gyration ($d\langle R_g^2\rangle/dT$) (a–c) and specific heat (C_v) (d–f) versus temperature for all types of block copolymer chains.

temperature, the relative shape anisotropy κ of all the models at T=0.5 was calculated and shown against chain stiffness k in Figure 9.

We can see that for homopolymers, κ monotonically increased with the increase of chain stiffness. Furthermore, the globule structure variations with increasing chain stiffness were similar among different types of homopolymer chains. For flexible homopolymers, the shape of the globule was spherical, while the globule turns to be prolate and oblate as the chain stiffness increases. For block copolymers, we can see that the symmetry of four types of polymer chains showed different characteristics in globule state. For linear block copolymer, κ monotonically increases with increasing chain stiffness, as in the case of homopolymer. For circular and 3_1 knot block copolymer chains, κ converges to the value of 0.25 as the chain stiffness increased, indicating that a planar symmetric chain configuration was dominant for stiff block copolymer. For 4_1 knot chains, κ first increased with increasing chain stiffness then slightly decreased in the case with k=8, meaning that another highly symmetric shape appeared for the block copolymer chain with the highest stiffness in this study.

Figure 10 shows typical configurations for all types of polymer chains at T=0.5. From the figure, the topological effect on the shape of polymer chains can be clearly observed.

5 Conclusions

In this study, we use molecular dynamics with integrated tempering sampling method to study the coil-to-globule transition of homopolymers and regularly distributed block copolymers with different topological constraint and chain stiffness. We found that the topological constraint and chain stiffness both play very important roles in the CG transition. Enhancing topological constraint results in effective excluded volume of the monomers, thus decreasing the CG transition temperature. The chain stiffness influences the polymer configurations at different temperatures. For semi-flexible homopolymers, an additional first-order like symmetry-broken transition emerges in the low temperature region. For block copolymer chains, the topological constraint does not change the transition temperatures much, but obviously reduces the structural and energetic signals of the CG transition.

The globule configurations at low temperatures for all types of polymer chains vary in shape and symmetry. For homopolymer chains with all types of topologies, the symmetry of the globule shape monotonically decreases with increasing chain stiffness. Block copolymer chains show very different relationship between the globule shape and the chain stiffness. Moreover, with increasing chain stiffness, knotted structures begin to show up for linear chains at low temperatures for both homopolymers and block copolymers (cf. Figure 10), which is consistent with those reported in literature.

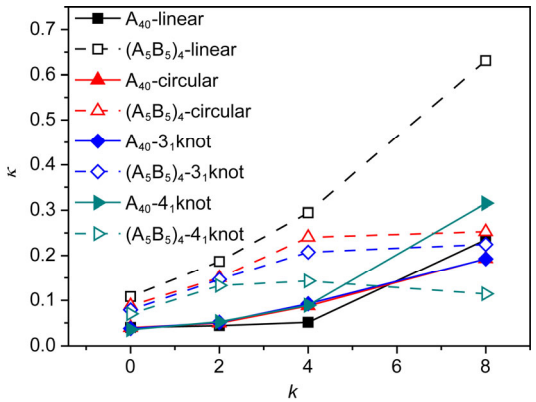

Figure 9 Relative shape anisotropy (κ) versus chain stiffness for both homopolymer and block copolymer chains.

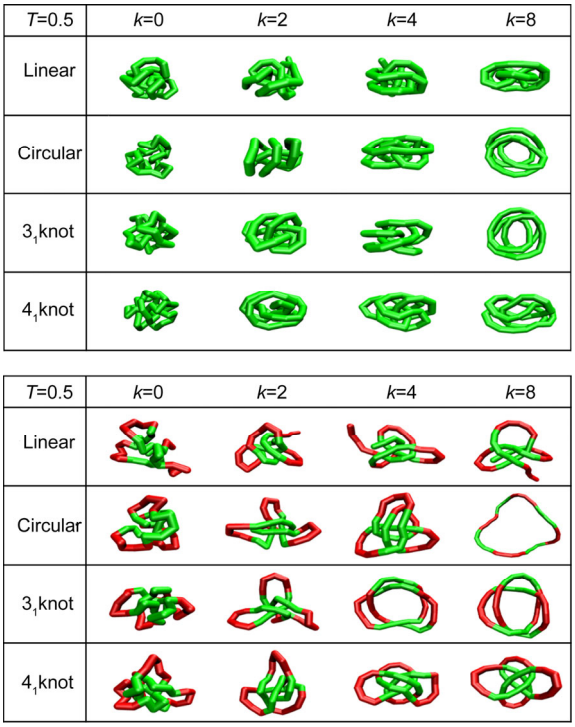

Figure 10 Typical configurations of all types of homopolymer and block copolymer chains at T=0.5.

This work was supported by the National Basic Research Program of China (2012CB821500), the National Natural Science Foundation of China (21025416), and Jilin Province Science and Technology Development Plan (20140519004JH). ZhongYuan Lu is also grateful to the Wenner-Gren Center Foundation for Scientific Research for financial support as visiting scientist in Sweden.

1 Dulbecco R, Vogt M. Evidence for a ring structure of polyoma virus DNA. *Proc Natl Acad Sci USA*, 1963, 50: 236–243
2 Vinogard J, Lebowitz J. Physical and topological properties of circular DNA. *J Gen Physiol,* 1966, 49: 103–125

3 Craik DJ, Daly NL, Bond T, Waine C. Plant cyclotides: a unique family of cyclic and knotted proteins that defines the cyclic cystine knot structural motif. *J Mol Biol*, 1999, 294: 1327–1336
4 Craik DJ, Conibear AC. The chemistry of cyclotides. *J Org Chem*, 2011, 76: 4805–4817
5 Mallam AL, Jackson SE. Folding studies on a knotted protein. *J Mol Biol*, 2005, 346: 1409–1421
6 Hsieh T. Knotting of the circular duplex DNA by type II DNA topoisomerase from Drosophila melanogaster. *J Biol Chem*, 1983, 258: 8413–8420
7 Trigueros S, Roca J. Production of highly knotted DNA by means of cosmid circularization inside phage capsids. *BMC Biotechnol*, 2007, 7: 94
8 Oike H. Supramolecular approach for synthesis and functionalization of cyclic macromolecules. *React Funct Polym*, 2007, 67: 1157–1167
9 Jia Z, Monteiro MJ. Cyclic polymers: methods and strategies. *J Polym Sci A*: *Polym Chem*, 2012, 50: 2085–2097
10 Xiong XQ, Yi C. Application of click chemistry in the synthesis of cyclic polymers. *Sci China Chem*, 2013, 43: 783–800
11 Ohta Y, Kushida Y, Matsushita Y, Takano A. SEC-MALS characterization of cyclization reaction products: formation of knotted ring polymer. *Polymer*, 2009, 50: 1297–1299
12 Ohta Y, Nakamura M, Matsushita Y, Takano A. Synthesis, separation and characterization of knotted ring polymers. *Polymer*, 2012, 53: 466–470
13 Cates ME, Deutsch JM. Conjectures on the statistics of ring polymers. *J Phys France*, 1986, 47: 2121–2128
14 Baiesi M, Orlandini E. Universal properties of knotted polymer rings. *Phys Rev E*, 2012, 86: 031805
15 Rosa A, Orlandini E, Tubiana L, Micheletti C. Structure and dynamics of ring polymers: entanglement effects because of solution density and ring topology. *Macromolecules*, 2011, 44: 8668–8680
16 Rawdon EJ, Kern JC, Piatek M, Plunkett P, Stasiak A, Millett KC. Effect of knotting on the shape of polymers. *Macromolecules*, 2008, 41: 8281–8287
17 Millett KC, Plunkett P, Piatek M, Rawdon EJ, Stasiak A. Effect of knotting on polymer shapes and their enveloping ellipsoids. *J Chem Phys*, 2009, 130: 165104
18 Rawdon E, Dobay A, Kern JC, Millett KC, Piatek M, Plunkett P, Stasiak A. Scaling behavior and equilibrium lengths of knotted polymers. *Macromolecules*, 2008, 41: 4444–4451
19 Kanaeda N, Deguchi T. Universality in the diffusion of knots. *Phy Rev E*, 2009, 79: 021806
20 Orlandini E, Stella AL, Vanderzande C, Zonta F. Slow topological time scale of knotted polymers. *J Phys A Math Theor*, 2008, 41: 122002
21 Narros A, Moreno AJ, Likos CN. Effects of knots on ring polymers in solvents of varying quality. *Macromolecules*, 2013, 46: 3654–3668
22 Chen WD, Chen JZ, Liu LJ, Xu XL, An LJ. Simulation study on conformational and dynamical properties of individual ring polymers in good solution. *Sci China Chem*, 2014, 44: 320–326
23 Ivanov VA, Paul W, Binder K. Finite chain length effects on the coil-globule transition of stiff-chain macromolecules: a Monte Carlo simulation. *J Chem Phys*, 1998, 109: 5659
24 Ivanov VA, Stukan MR, Vasilevskaya VV, Paul W, Binder K. Structures of stiff macromolecules of finite chain length near the coil-globule transition: a Monte Carlo simulation. *Macromol Theor Simul*, 2000, 9: 488–499
25 Bachmann M, Janke W. Thermodynamics of lattice heteropolymers. *J Chem Phys*, 2004, 120: 6779–6791
26 Bachmann M, Arkın H, Janke W. Multicanonical study of coarse-grained off-lattice models for folding heteropolymers. *Phys Rev E*, 2005, 71: 031906
27 Wang L, Chen T, Lin X, Liu Y, Liang H. Canonical and microcanonical analysis of nongrafted homopolymer adsorption by an attractive substrate. *J Chem Phys*, 2009, 131: 244902
28 Chen T, Wang L, Lin X, Liu Y, Liang H. Microcanonical analysis of adsorption of homopolymer chain on a surface. *J Chem Phys*, 2009, 130: 244905
29 Wang Z, He X. Phase transition of a single star polymer: a Wang-Landau sampling study. *J Chem Phys*, 2011, 135: 094902
30 Guo J, Liang H, Wang ZG. Coil-to-globule transition by dissipative particle dynamics simulation. *J Chem Phys*, 2011, 134: 244904
31 Seaton DT, Schnabel S, Landau DP, Bachmann M. From flexible to stiff: systematic analysis of structural phases for single semiflexible polymers. *Phys Rev Lett*, 2013, 110: 028103
32 Arkin H, Janke W. Gyration tensor based analysis of the shapes of polymer chains in an attractive spherical cage. *J Chem Phys*, 2013, 138: 054904
33 Wang Z, Wang L, He X. Phase transition of a single protein-like copolymer chain. *Soft Matter*, 2013, 9: 3106
34 Chi P, Wang Z, Yin Y, Li BH, Shi AC. Finite-length effects on the coil-globule transition of a strongly charged polyelectrolyte chain in a salt-free solvent. *Phy Rev E*, 2013, 87: 042608
35 Wang W, Zhao P, Yang X, Lu ZY. Coil-to-globule transitions of homopolymers and multiblock copolymers. *J Chem Phys*, 2014, 141: 244907
36 Swetnam A, Brett C, Allen MP. Phase diagrams of knotted and unknotted ring polymers. *Phys Rev E*, 2012, 85: 031804
37 Zhao Y, Ferrari F. A numerical technique for studying topological effects on the thermal properties of knotted polymer rings. *J Stat Mech-Theory E*, 2012: P11022
38 Zhao Y, Ferrari F. A study of polymer knots using a simple knot invariant consisting of multiple contour integrals. *J Stat Mech-Theory E*, 2013: P10010
39 Yang L, Gao YQ. A selective integrated tempering method. *J Chem Phys*, 2009, 131: 214109
40 Yang L, Shao Q, Gao YQ. Comparison between integrated and parallel tempering methods in enhanced sampling simulations. *J Chem Phys*, 2009, 130: 124111
41 Zhao P, Yang LJ, Gao YQ, Lu ZY. Facile implementation of integrated tempering sampling method to enhance the sampling over a broad range of temperatures. *Chem Phys*, 2013, 415: 98–105
42 Zhu YL, LiuH, Li ZW, Qian HJ, Milano G, Lu ZY. GALAMOST: GPU-accelerated large-scale molecular simulation toolkit. *J Comput Chem*, 2013, 34: 2197–2211
43 Roovers J, Toporowski PM. Synthesis of high molecular weight ring polystyrenes. *Macromolecules*, 1983, 16: 843–849
44 Roovers J. Dilute-solution properties of ring polystyrenes. *J Polym Sci Polym Phys Ed*, 1985, 23: 1117–1126
45 Takano A, Kushida Y, Ohta Y, Masuoka K, Matsushita Y. The second virial coefficients of highly-purified ring polystyrenes in cyclohexane. *Polymer*, 2009, 50: 1300–1303
46 des Cloizeaux J. Ring polymers in solution: topological effects. *J Phys Lett*, 1981, 42: L-433
47 Tanaka F. Osmotic pressure of ring-polymer solutions. *J Chem Phys*, 1987, 87: 4201
48 Iwata K. θ temperature of ring polymers: another evidence of topological interaction. *Macromolecules*, 1989, 22: 3702–3706